Centrum voor Wiskunde en Informatica
Centre for Mathematics and Computer Science

B. Koren, P.W. Hemker

Damped, direction-dependent multigrid for hypersonic flow computations

Department of Numerical Mathematics Report NM-R8922 November

The Centre for Mathematics and Computer Science is a research institute of the Stichting Mathematisch Centrum, which was founded on February 11, 1946, as a nonprofit institution aiming at the promotion of mathematics, computer science, and their applications. It is sponsored by the Dutch Government through the Netherlands Organization for the Advancement of Research (N.W.O.).

Copyright © Stichting Mathematisch Centrum, Amsterdam

Damped, Direction-Dependent Multigrid for Hypersonic Flow Computations

B. Koren and P.W. Hemker
Centre for Mathematics and Computer Science
P.O. Box 4079, 1009 AB Amsterdam, The Netherlands

A nonlinear multigrid technique with improved robustness is developed for the solution of the steady Euler equations. The system of nonlinear equations is discretized by an upwind finite volume method. Collective symmetric point Gauss-Seidel relaxation is applied as the standard smoothing technique. In case of failure of the point relaxation, a switch is made to a local evolution technique. The novel robustness improvements to the nonlinear multigrid method are a local damping of the restricted defect, and a global upwind prolongation of the correction. The defect damping is derived from a two-grid convergence analysis. The upwind prolongation makes efficient use of the P-variant of Osher's approximate Riemann solver. Satisfactory convergence results are shown for the computation of a hypersonic launch and reentry flow around a blunt forebody with canopy. For the test cases considered, it appears that the improved multigrid method performs significantly better than a standard nonlinear multigrid method.

1980 Mathematics Subject Classification: 65H10, 65N10, 65N20, 76K05, 76N10.
Key Words and Phrases: nonlinear multigrid method, steady Euler equations, hypersonic flows.
Note: This work was supported by the European Space Agency (ESA), through Avions Marcel Dassault - Bréguet Aviation (AMD-BA).

1. Introduction

1.1. Governing equations

The flow equations considered are the steady, 2D Euler equations

$$\frac{\partial}{\partial t}\begin{bmatrix}\rho\\ \rho u\\ \rho v\\ \rho e\end{bmatrix}+\frac{\partial}{\partial x}\begin{bmatrix}\rho u\\ \rho u^2+p\\ \rho uv\\ \rho u(e+\frac{p}{\rho})\end{bmatrix}+\frac{\partial}{\partial y}\begin{bmatrix}\rho v\\ \rho vu\\ \rho v^2+p\\ \rho v(e+\frac{p}{\rho})\end{bmatrix}=0, \tag{1.1a}$$

with the total energy satisfying, assuming a perfect gas,

$$e=\frac{1}{\gamma-1}\frac{p}{\rho}+\frac{1}{2}(u^2+v^2). \tag{1.1b}$$

So far, real gas effects are not taken into account. The specific heat ratio γ of the di-atomic gas considered is assumed to be constant and determined by fully excited translational and rotational energies only. (Though it could easily be replaced by a function ranging from zero up to the full equipartition value, the vibrational energy is assumed to be zero.)

1.2. Existing computational method

For a description of the existing computational method which is taken as a point of departure, we refer to [2] and [3]. Here we give an overview of its main characteristics only.

Discretization method. Discretized equations are obtained by dividing the computational domain Ω into quadrilateral finite volumes $\Omega_{i,j}$, and by requiring that the conservation laws, (1.1a) in integral form, hold for each finite volume separately. This discretization requires an evaluation of the convective flux vector at each cell face. For this, we prefer an upwind approach which follows the Godunov principle [1]. The 1D Riemann problem thus arising at each cell face is solved in an approximate way by using Osher's scheme [4] in its P-variant [2]. The left and right state in the 1D Riemann problem (which determine the accuracy of the convective discretization) are simply taken equal to those in the corresponding adjacent volumes, leading to first-order accuracy.

Solution method. For the solution of the nonlinear system of first-order accurate discretized Euler equations, we apply collective symmetric point Gauss-Seidel relaxation, accelerated by nonlinear multigrid. The solution process is started by nested iteration. In the relaxation method one or more exact Newton steps are used for the collective update of the four state vector components in each finite volume. The method summarized so far is that presented in [2]. The possible extension, as presented in [3], is the following. If necessary, the success (or failure) of the relaxation method may be continuously checked by monitoring the error behaviour and the physical relevance of the iterates. In case of failure of the relaxation method, a switch is made to a fully explicit evolution technique to solve the system of nonlinear equations in the particular cell where problems arise. This solution method with enhanced robustness still does not require any tuning of parameters. We proceed by giving a summary of our nonlinear multigrid and nested iteration method.

Nested grids are applied such that each finite volume on a coarse grid is the union of 2×2 volumes on the next finer grid. Let $\Omega_1,...,\Omega_{l-1},\Omega_l,\Omega_{l+1},...,\Omega_L$ be a sequence of such nested grids, with Ω_1 the coarsest and Ω_L the finest grid, and let $N_l(q_l)=r_l$ denote the nonlinear system of first-order discretized Euler equations on Ω_l, with r_l a possibly non-zero right-hand side related to the multigrid iteration. Then a single nonlinear multigrid cycle and the nested iteration, as applied in our existing solution method, are defined in the following way.

Nonlinear multigrid iteration:
- Apply on Ω_l p pre-relaxation sweeps to $N_l(q_l)=r_l$.
- Compute the defect $d_l=N_l(q_l)-r_l$, and restrict it to Ω_{l-1}: $d_{l-1}=I_l^{l-1}d_l$, where I_l^{l-1} is a restriction operator for right-hand sides.
- Compute on the next coarser grid Ω_{l-1} the right-hand side $r_{l-1}=N_{l-1}(q_{l-1})-d_{l-1}$. For the initial estimate of q_{l-1}, we use the latest obtained q_{l-1}.
- Approximate the solution of $N_{l-1}(q_{l-1})=r_{l-1}$ by the application of σ nonlinear multigrid cycles. Denote the approximation obtained as $\tilde{q}_{l-1}$.
- Correct the current solution by $q_l=q_l+\tilde{I}_{l-1}^l(\tilde{q}_{l-1}-q_{l-1})$, where $\tilde{I}_{l-1}^l$ is a linear prolongation operator for solutions.
- Apply on Ω_l q post-relaxation sweeps to $N_l(q_l)=r_l$.

For $l=1$, the coarse grid correction is skipped of course. For the restriction operator I_l^{l-1} and the prolongation operator $\tilde{I}_{l-1}^l$ we take

$$(r_{l-1})_{i,j} = (I_l^{l-1}r_l)_{i,j} = (r_l)_{2i-1,2j-1}+(r_l)_{2i-1,2j}+(r_l)_{2i,2j-1}+(r_l)_{2i,2j}, \tag{1.2a}$$

$$(\tilde{I}_{l-1}^l q_{l-1})_{2i-1,2j-1} = (\tilde{I}_{l-1}^l q_{l-1})_{2i-1,2j} = (\tilde{I}_{l-1}^l q_{l-1})_{2i,2j-1} = (\tilde{I}_{l-1}^l q_{l-1})_{2i,2j} = (q_{l-1})_{i,j}. \tag{1.2b}$$

If not mentioned otherwise, for σ, and p and q we use at each level l: $\sigma=1$, and $p=q=1$; i.e. as nonlinear multigrid cycles we use V-cycles with a single pre- and one post-relaxation sweep per level.

Nested iteration:
- Choose a (possibly crude) initial estimate q_1.
- Improve q_1 by a single nonlinear multigrid cycle as just defined above.
- Prolongate the improved approximation q_1 to Ω_2, yielding an initial estimate for q_2.
- Improve q_2 by a single nonlinear multigrid cycle as defined above.
- Continue the previous process until an initial estimate for q_L has been obtained by prolongation of q_{L-1}.

The prolongation operator for obtaining the first approximation on each next finer grid may be the piecewise constant operator (1.2b) or - preferably - a more accurate operator (for instance a bilinear operator).

1.3. Results

To give a quick impression of the performance of our existing multigrid method, we consider: (i) the NACA0012-airfoil at $M_\infty=0.63$, $\alpha=2^0$ (smooth subsonic flow) and at $M_\infty=0.85$, $\alpha=1^0$ (non-smooth transonic flow), and (ii) a blunt forebody with canopy at $M_\infty=8.15$, $\alpha=0^0$ (non-smooth hypersonic flow). For details about the geometry of the latter body, we refer to [3].

As finest finest-grid for the NACA0012-airfoil we consider the 128×32 O-type grid given in Fig. 1.

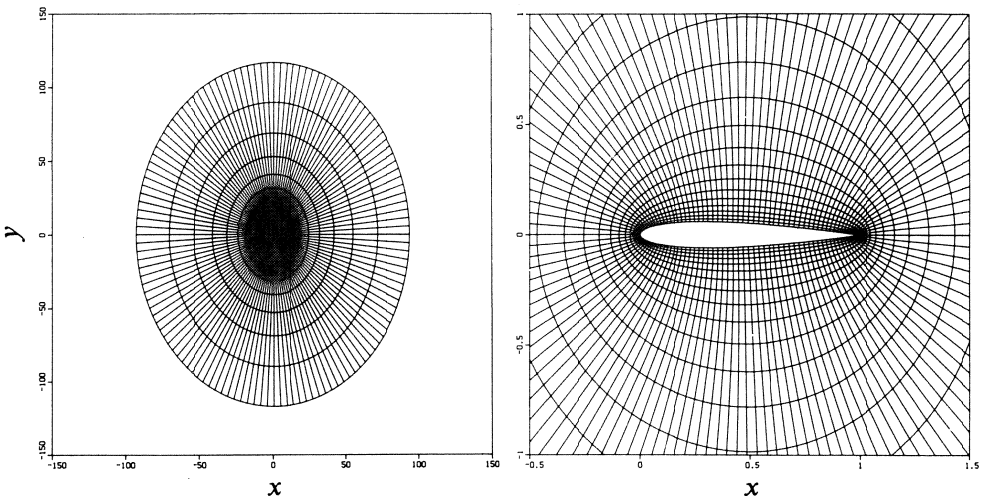

a. In full. b. In detail.

Fig. 1. 128×32-grid (Ω_5) NACA0012-airfoil.

For the blunt body, as finest finest-grid so far, we consider the 64×32 C-type grid given in Fig. 2.

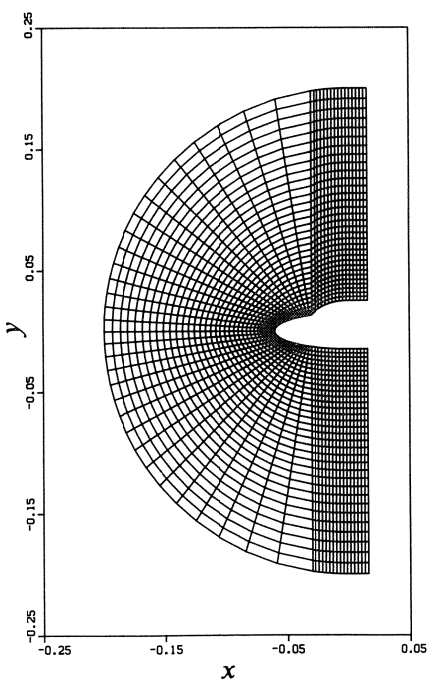

Fig. 2. 64×32-grid (Ω_5) blunt forebody with canopy.

1.3.1. Smooth subsonic and non-smooth transonic flow. For the NACA0012-flows we obtain the multigrid performance given in Fig. 3. In both graphs, the residual ratio along the vertical axis is the ratio $\Sigma_{k=1}^{4}|(N_L(q_L^n))_k|/\Sigma_{k=1}^{4}|(N_L(q_L^1))_k|$, $L=3,4,5$ versus the number of cycles performed, one multigrid cycle being a V-cycle with $p=q=1$, $\forall l$, and, for Ω_5 only, one single-grid cycle being the equivalent number of finest-grid relaxation sweeps. $|(N_L(q_L^n))_k|$ denotes the summation - over all volumes at Ω_L - of the absolute values of the k-th component in the first-order Euler defects, with q_L^n denoting the solution at Ω_L after the n-th multi- or single-grid cycle. Considering the single-grid convergence histories, for both the smooth subsonic case and the non-smooth transonic case, the effectiveness of the multigrid method is clear.

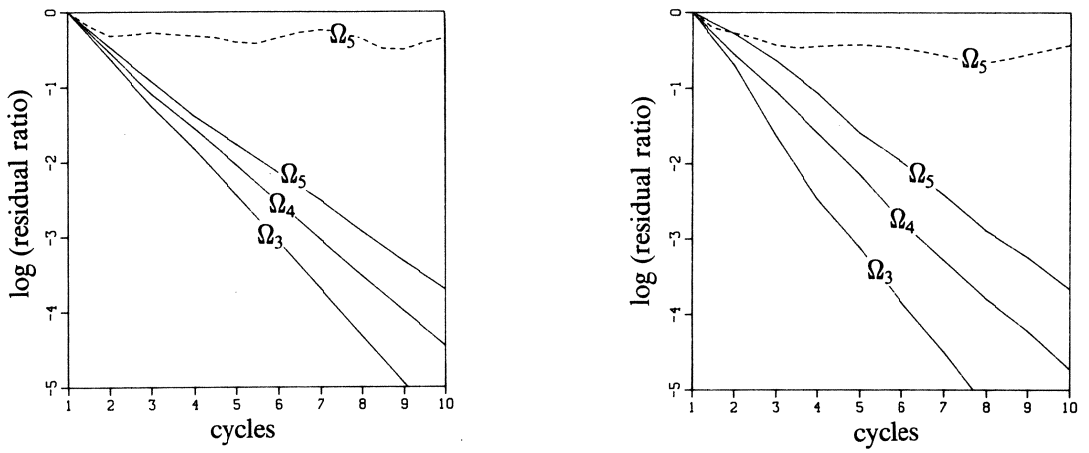

a. At $M_\infty=0.63$, $\alpha=2^0$. b. At $M_\infty=0.85$, $\alpha=1^0$.

Fig. 3. Multigrid behaviours NACA0012-airfoil
(------ : single-grid, —— : multigrid).

1.3.2. Non-smooth hypersonic flow. For both previous airfoil flows, the switched-relaxation-evolution technique does not need to be invoked. However, for the hypersonic blunt body flow, the latter technique must be used. (Without this technique, already in the first relaxation sweep on the coarsest grid, the solution process breaks down.) For a similar hypersonic flow, in [3] we have already presented single-grid convergence results obtained with the switched-relaxation-evolution approach. With this approach, for all cases considered in [3] we obtain convergence. Further, it appears - as was expected - that the evolution technique makes itself superfluous in the course of the iteration process. For the present hypersonic test case, we have the same single-grid experience. Unfortunately, with the switched-relaxation-evolution technique combined with the existing multigrid method, no satisfactory results are obtained; see Fig. 4, with q_L^0 being the approximate solution obtained by the nested iteration. Standard changes to the multigrid algorithm, such as for instance the replacement of V-cycles by W-cycles do not help. In the next section we present novel changes to the multigrid algorithm which will improve the poor results presented in Fig. 4.

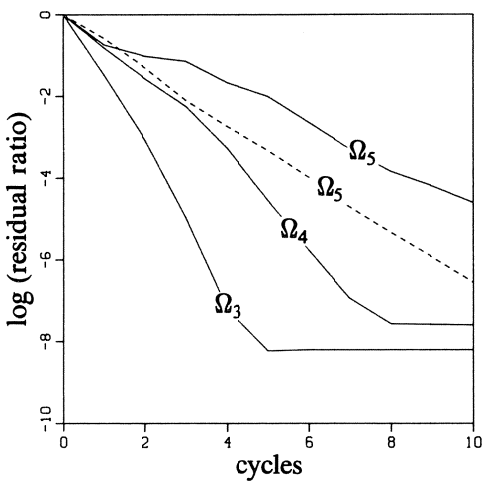

Fig. 4. Multigrid convergence behaviour blunt forebody with canopy at $M_\infty=8.15$, $\alpha=0^0$
(------ : single-grid —— : multigrid)

2. IMPROVED MULTIGRID METHOD

Applying multigrid in the standard way as described in section 1.2, we experience that for hypersonic test cases, local coarse-to-fine grid corrections may be transferred which sweep the corresponding fine grid iterates out of the attraction domain of the pure relaxation technique, and even out of that of the switched-relaxation-evolution technique. The cause of these problems may be either the coarse grid corrections themselves, or the prolongation operator, or the combination of both. Therefore, in the present paper, to avoid possibly bad coarse grid corrections, we present a local damping technique for the restricted defects, and hence - implicitly - a local damping technique for the coarse grid corrections. To avoid a possibly bad correction transfer, we present an alternative prolongation: a direction-dependent prolongation.

2.1. Defect damping

In [6], De Zeeuw reports a serious lack of robustness of standard nonlinear multigrid applied to a test case described by the steady, 1D semiconductor equations. De Zeeuw meets the quest for greater robustness by a local damping of the restricted defect. Though the way in which this damping is introduced in [6] is not yet very convincing from a theoretical point of view (only very little evidence is given for the amount of damping to be applied), it certainly is convincing from an experimental point of view. It leads to a significantly more robust multigrid method. For a class of elliptic problems, a likewise successful, but basically different damping technique for improving the robustness of nonlinear multigrid, is that proposed by Reusken [5]. Instead of locally damping the restricted defect, Reusken proposes to damp globally (i.e. uniformly) the coarse grid correction, the amount of damping to be applied being prescribed by fairly rigorous theory. For the present hypersonic flow computations, we prefer the type of damping as proposed by De Zeeuw, this (i) because it is not restricted to a specific class of elliptic problems (not even to elliptic problems in general), (ii) because of its a-priori character (a-posteriori damping like that in [5] may already be too late), and (iii) because of its local application (global damping like that in [5] may strongly reduce the positive effects of the coarse grid correction).

The local defect damping to be applied is now introduced by deriving the two-grid amplification operator. Let

$$N_l(q_l) = r_l \tag{2.1}$$

denote a nonlinear system of fine grid equations that we want to solve. Then the corresponding $(n+1)$-th coarse grid problem $(n=0,1,...,N)$ to be solved, reads

$$N_{l-1}(q_{l-1}^{n+1}) = N_{l-1}(q_{l-1}^{n}) - S_{l-1} I_l^{l-1}(N_l(q_l^{n+\frac{1}{3}}) - r_l), \quad n=0,1,...,N, \tag{2.2}$$

with S_{l-1} denoting the operator for the defect damping, with $q_l^{n+\frac{1}{3}}$ denoting the fine grid iterate as obtained after the (fine grid) pre-relaxation, and with q_{l-1}^{n} and q_{l-1}^{n+1} denoting the coarse grid iterates before the (coarse grid) pre-relaxation and after the (coarse grid) post-relaxation, respectively. With (2.1), and by linearization (neglecting higher-order terms), from (2.2) we derive the relation

$$q_{l-1}^{n+1} - q_{l-1}^{n} = -\left[\frac{dN_{l-1}(q_{l-1}^{n})}{dq_{l-1}}\right]^{-1} S_{l-1} I_l^{l-1} \frac{dN_l(q_l^{n+\frac{1}{3}})}{dq_l}(q_l^{n+\frac{1}{3}} - q_l^{*}), \quad n=0,1,...,N, \tag{2.3}$$

in which q_l^{*} denotes the fully converged solution of (2.1). Considering for the coarse grid correction $q_{l-1}^{n+1} - q_{l-1}^{n}$ also the relation

$$\tilde{I}_{l-1}^{l}(q_{l-1}^{n+1} - q_{l-1}^{n}) = (q_l^{n+\frac{2}{3}} - q_l^{n+\frac{1}{3}}), \quad n=0,1,...,N, \tag{2.4}$$

with $q_l^{n+\frac{2}{3}}$ denoting the fine grid iterate before the (fine grid) post-relaxation, it follows the two-grid convergence result

$$q_l^{n+\frac{2}{3}} - q_l^{*} = \left[I_l - \tilde{I}_{l-1}^{l}\left[\frac{dN_{l-1}(q_{l-1}^{n})}{dq_{l-1}}\right]^{-1} S_{l-1} I_l^{l-1} \frac{dN_l(q_l^{n+\frac{1}{3}})}{dq_l}\right](q_l^{n+\frac{1}{3}} - q_l^{*}), \quad n=0,1,...,N, \tag{2.5}$$

in which I_l denotes the identity operator on Ω_l. From (2.5), it is clear that in case the property

$$\frac{dN_{l-1}(q_{l-1}^{n})}{dq_{l-1}} = I_l^{l-1} \frac{dN_l(q_l^{n+\frac{1}{3}})}{dq_l} \tilde{I}_{l-1}^{l} \tag{2.6}$$

is satisfied, (2.5) implies

$$I_l^{l-1}\frac{dN_l(q_l^{n+\frac{1}{3}})}{dq_l}(q_l^{n+\frac{1}{3}}-q_l^*) = (I_{l-1}-S_{l-1})I_l^{l-1}\frac{dN_l(q_l^{n+\frac{1}{3}})}{dq_l}(q_l^{n+\frac{1}{3}}-q_l^*),\quad n=0,1,...,N, \tag{2.7}$$

indicating that for optimal two-grid convergence no damping should be applied ($S_{l-1}=I_{l-1}$). However, in hypersonic flow computations, q_{l-1}^n and $q_l^{n+\frac{1}{3}}$ may strongly differ from each other, and as a consequence also both Jacobians. For example, a hypersonic shock wave which is detached on Ω_l, may easily be attached on Ω_{l-1}, with as a probable consequence that there, locally, (2.6) is not satisfied at all. If (2.6) is not satisfied, in particular if this is only very locally the case, damping of the restricted defect at those places might be very useful. For optimal two-grid convergence, from (2.5) we derive as local damping factor for the defect in finite volume $(\Omega_{l-1})_{i,j}$, to be applied in the $(n+1)$-th multigrid cycle:

$$(S_{l-1}^{n+1})_{i,j} = \min\left[1,\frac{\|(N'_{l-1})_{i,j}\|}{\max\left[\|(N'_l)_{2i-1,2j-1}\|,\|(N'_l)_{2i-1,2j}\|,\|(N'_l)_{2i,2j-1}\|,\|(N'_l)_{2i,2j}\|\right]}\right],\quad n=0,1,...,N, \tag{2.8}$$

with $N'_{l-1}\equiv dN_{l-1}(q_{l-1}^n)/dq_{l-1}$, with $N'_l\equiv dN_l(q_l^{n+\frac{1}{3}})/dq_l$, and with $\|\ \|$ some matrix norm. Notice that the local damping factor (2.8) is more or less the 2D equivalent of the 1D damping introduced in [6]. To see if some additional gain can be obtained by also allowing local defect amplification, in a numerical experiment we will also consider

$$(S_{l-1}^{n+1})_{i,j} = \frac{\|(N'_{l-1})_{i,j}\|}{\max\left[\|(N'_l)_{2i-1,2j-1}\|,\|(N'_l)_{2i-1,2j}\|,\|(N'_l)_{2i,2j-1}\|,\|(N'_l)_{2i,2j}\|\right]},\quad n=0,1,...,N. \tag{2.9}$$

At convergence of the solution, the defect multiplication, both in case of (2.8) and in case of (2.9), will also have converged. However, as opposed to e.g. the correction damping proposed in [5], the present multiplication will not have vanished at convergence, neither in case of (2.8), nor in case of (2.9).

2.2. *Direction-dependent grid transfer operators*

2.2.1. Prolongation. The standard, piecewise constant correction prolongation may be illustrated as in Fig. 5.

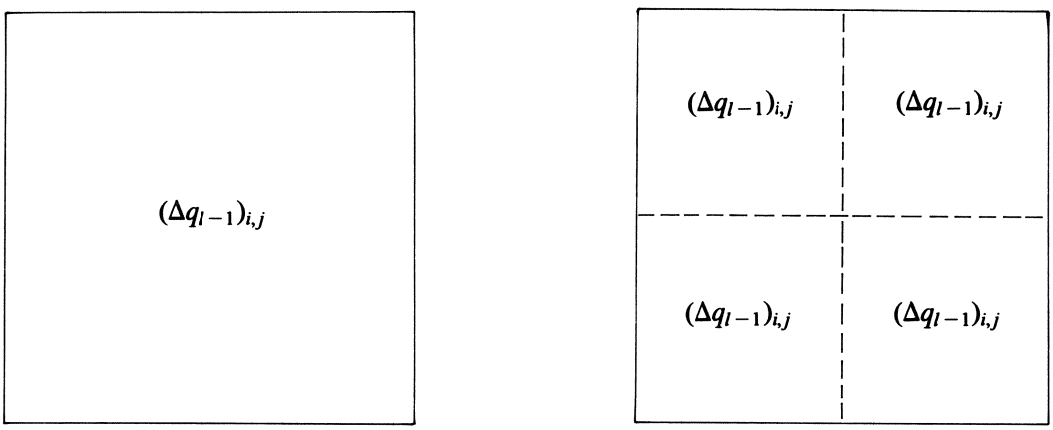

a. $(\Omega_{l-1})_{i,j}$. b. $(\Omega_l)_{2i-1,2j-1}, (\Omega_l)_{2i-1,2j}, (\Omega_l)_{2i,2j-1}, (\Omega_l)_{2i,2j}$.

Fig. 5. Coarse grid finite volume with corresponding next-finer grid volumes, and corresponding piecewise constant corrections.

In mathematical terms, solution correction by means of the piecewise constant correction prolongation may be written as

$$\begin{aligned}
(q_l^{\text{new}})_{2i-1,2j-1} &= (q_l^{\text{old}})_{2i-1,2j-1} + (\Delta q_{l-1})_{i,j},\\
(q_l^{\text{new}})_{2i-1,2j} &= (q_l^{\text{old}})_{2i-1,2j} + (\Delta q_{l-1})_{i,j},\\
(q_l^{\text{new}})_{2i,2j-1} &= (q_l^{\text{old}})_{2i,2j-1} + (\Delta q_{l-1})_{i,j},\\
(q_l^{\text{new}})_{2i,2j} &= (q_l^{\text{old}})_{2i,2j} + (\Delta q_{l-1})_{i,j},
\end{aligned} \tag{2.10a}$$

with

$$(\Delta q_{l-1})_{i,j} = (q_{l-1}^{\text{new}})_{i,j} - (q_{l-1}^{\text{old}})_{i,j}. \tag{2.10b}$$

The direction-dependent correction prolongation that we propose now can be illustrated as in Fig. 6.

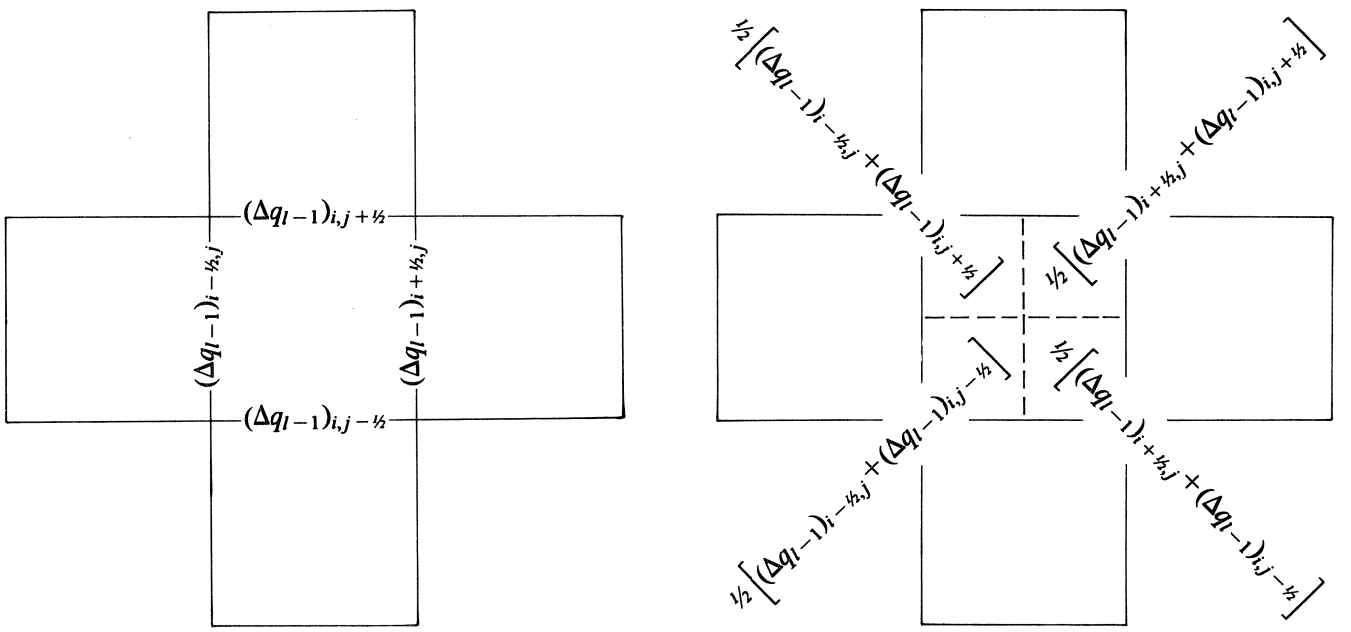

a. $(\Omega_{l-1})_{i,j}$.

b. $(\Omega_l)_{2i-1,2j-1}, (\Omega_l)_{2i-1,2j}, (\Omega_l)_{2i,2j-1}, (\Omega_l)_{2i,2j}$.

Fig. 6. Coarse grid finite volume with corresponding next-finer grid volumes, and corresponding direction-dependent corrections.

In mathematical terms - analogous to (2.10) - solution correction by means of this direction-dependent prolongation is written as

$$\begin{aligned}
(q_l^{\text{new}})_{2i-1,2j-1} &= (q_l^{\text{old}})_{2i-1,2j-1} + (\Delta q_{l-1})_{2i-1,2j-1},\\
(q_l^{\text{new}})_{2i-1,2j} &= (q_l^{\text{old}})_{2i-1,2j} + (\Delta q_{l-1})_{2i-1,2j},\\
(q_l^{\text{new}})_{2i,2j-1} &= (q_l^{\text{old}})_{2i,2j-1} + (\Delta q_{l-1})_{2i,2j-1},\\
(q_l^{\text{new}})_{2i,2j} &= (q_l^{\text{old}})_{2i,2j} + (\Delta q_{l-1})_{2i,2j},
\end{aligned} \tag{2.11a}$$

with the four corrections defined as centred averages of the coarse grid cell face corrections:

$$\begin{aligned}
(\Delta q_{l-1})_{2i-1,2j-1} &= \tfrac{1}{2}\left[(\Delta q_{l-1})_{i-\frac{1}{2},j} + (\Delta q_{l-1})_{i,j-\frac{1}{2}}\right],\\
(\Delta q_{l-1})_{2i-1,2j} &= \tfrac{1}{2}\left[(\Delta q_{l-1})_{i-\frac{1}{2},j} + (\Delta q_{l-1})_{i,j+\frac{1}{2}}\right],\\
(\Delta q_{l-1})_{2i,2j-1} &= \tfrac{1}{2}\left[(\Delta q_{l-1})_{i+\frac{1}{2},j} + (\Delta q_{l-1})_{i,j-\frac{1}{2}}\right],\\
(\Delta q_{l-1})_{2i,2j} &= \tfrac{1}{2}\left[(\Delta q_{l-1})_{i+\frac{1}{2},j} + (\Delta q_{l-1})_{i,j+\frac{1}{2}}\right],
\end{aligned} \tag{2.11b}$$

and with the coarse grid cell face corrections defined by

$$\begin{aligned}
(\Delta q_{l-1})_{i-\frac{1}{2},j} &= (q_{l-1}^{\text{new}})_{i-\frac{1}{2},j} - (q_{l-1}^{\text{old}})_{i-\frac{1}{2},j}, \\
(\Delta q_{l-1})_{i+\frac{1}{2},j} &= (q_{l-1}^{\text{new}})_{i+\frac{1}{2},j} - (q_{l-1}^{\text{old}})_{i+\frac{1}{2},j}, \\
(\Delta q_{l-1})_{i,j-\frac{1}{2}} &= (q_{l-1}^{\text{new}})_{i,j-\frac{1}{2}} - (q_{l-1}^{\text{old}})_{i,j-\frac{1}{2}}, \\
(\Delta q_{l-1})_{i,j+\frac{1}{2}} &= (q_{l-1}^{\text{new}})_{i,j+\frac{1}{2}} - (q_{l-1}^{\text{old}})_{i,j+\frac{1}{2}},
\end{aligned} \tag{2.11c}$$

where the cell face states are computed in an upwind manner. We notice that instead of the present procedure of computing coarse grid cell face states in an upwind manner, and from that, in a centred manner, fine grid cell centre states, might as well have been the reverse: computing the coarse grid cell face states in a *centred* manner, and from that the fine grid cell centre states in an *upwind* manner. However, a drawback of the latter approach is that it requires additional geometrical data for the upwind computation of the fine grid cell centre states.
Given a left and right cell face state (q_{left} and q_{right}), for a general 1D upwind scheme, a cell face state q_{face} may be computed from

$$f(q_{\text{face}}) = F(q_{\text{left}}, q_{\text{right}}), \tag{2.12}$$

where $f(q)$ and $F(q_{\text{left}}, q_{\text{right}})$ denote the exact and numerical Euler flux function, respectively. A drawback of the Euler equations is that obtaining a primitive state vector like e.g. $q=(\rho,u,v,p)^T$ from $f(q)=(\rho u, \rho u^2+p, \rho uv, \rho u(e+p/\rho))^T$ requires the solution of a quadratic algebraic equation. Fortunately, with the P-variant of Osher's scheme [2], for most Riemann-problem cases arising in aeronautics $F(q_{\text{left}}, q_{\text{right}})=f(q_*)$, q_* being a well-defined, *single* state vector on the Osher path, connecting q_{left} and q_{right} in state space. Hence, with the P-variant, in most cases - without evaluating $F(q_{\text{left}}, q_{\text{right}})$ - we can directly identify q_{face} as $q_{\text{face}}=q_*$. For the O-variant of Osher's scheme [2], in almost all Riemann-problem cases arising in aeronautics $F(q_{\text{left}}, q_{\text{right}})$ is found to be the sum of three different fluxes $f(q)$. In these cases, because of $f(q)$'s nonlinearity, the previous simple procedure is not possible. In the (rare) cases where the P-variant also leads to a sum of fluxes, we solve the quadratic equation and in case of a positive discriminant, and one zero being physically irrelevant (negative ρ and/or p), we take the zero which is physically relevant (positive ρ and p). In all other cases, we simply take $q_{\text{face}}=\frac{1}{2}(q_{\text{left}}+q_{\text{right}})$. Because of the consistency of Osher's scheme at boundaries, there the present upwind prolongation can also be applied in a consistent way. To conclude, we remark that the upwind prolongation may lead to cell face states which are local extrema in state space.

2.2.2. Restriction. A provable consequence of the upwind prolongation is that - unfortunately - no restriction operator I_l^{l-1} can be made for which the coarse grid finite volume discretization is a formal Galerkin approximation of the fine grid finite volume discretization [2]. The possibly most effective restriction operator that can be really made is the exact adjoint of the nonlinear prolongation operator. Unfortunately - as opposed to the upwind prolongation - the exactly adjoint restriction operator will certainly lead to a significant increase of the computational overhead. More suitable seems to be a linear approximation of the exact (nonlinear) adjoint. For this we write the latest obtained coarse grid cell face states as linear combinations of the corresponding left and right states:

$$(q_{\text{face}})_k = a_k(q_{\text{left}})_k + (1-a_k)(q_{\text{right}})_k, \quad k=1,2,3,4, \tag{2.13a}$$

$$a_k = \frac{(q_{\text{face}})_k/(q_{\text{right}})_k - 1 + \epsilon/2}{(q_{\text{left}})_k/(q_{\text{right}})_k - 1 + \epsilon}, \quad \epsilon \ll 1, \tag{2.13b}$$

where q is the conservative state vector, $q=(\rho,\rho u,\rho v,\rho e)^T$, and ϵ a small parameter which guarantees that $(q_{\text{face}})_k$ is a central average in case $(q_{\text{left}})_k=(q_{\text{right}})_k=(q_{\text{face}})_k$. With next the centred computation of the fine grid cell centre states, we then have

$$(q_l)_{2i-1,2j-1,k} = (\tilde{I}_{l-1}^{l} q_{l-1})_{2i-1,2j-1,k} = \tfrac{1}{2}\,(a_{l-1})_{i-\frac{1}{2},j,k}\,(q_{l-1})_{i-1,j,k} + \tfrac{1}{2}\left[2-(a_{l-1})_{i-\frac{1}{2},j,k}-(a_{l-1})_{i,j-\frac{1}{2},k}\right](q_{l-1})_{i,j,k} + \tfrac{1}{2}\,(a_{l-1})_{i,j-\frac{1}{2},k}\,(q_{l-1})_{i,j-1,k}\,, \quad k=1,2,3,4, \tag{2.14a}$$

$$(q_l)_{2i-1,2j,k} = (\tilde{I}_{l-1}^{l} q_{l-1})_{2i-1,2j,k} = \tfrac{1}{2}\,(a_{l-1})_{i-\frac{1}{2},j,k}\,(q_{l-1})_{i-1,j,k} + \tfrac{1}{2}\left[1-(a_{l-1})_{i-\frac{1}{2},j,k}+(a_{l-1})_{i,j+\frac{1}{2},k}\right](q_{l-1})_{i,j,k} + \tfrac{1}{2}\left[1-(a_{l-1})_{i,j+\frac{1}{2},k}\right](q_{l-1})_{i,j+1,k}\,, \quad k=1,2,3,4, \tag{2.14b}$$

$$(q_l)_{2i,2j-1,k} = (\tilde{I}_{l-1}^{l} q_{l-1})_{2i,2j-1,k} = \tfrac{1}{2}\left[1-(a_{l-1})_{i+\frac{1}{2},j,k}\right](q_{l-1})_{i+1,j,k} + \tfrac{1}{2}\left[1+(a_{l-1})_{i+\frac{1}{2},j,k}-(a_{l-1})_{i,j-\frac{1}{2},k}\right](q_{l-1})_{i,j,k} + \tfrac{1}{2}\,(a_{l-1})_{i,j-\frac{1}{2},k}\,(q_{l-1})_{i,j-1,k}\,, \quad k=1,2,3,4, \tag{2.14c}$$

$$(q_l)_{2i,2j,k} = (\tilde{I}_{l-1}^{l} q_{l-1})_{2i,2j,k} = \tfrac{1}{2}\left[1-(a_{l-1})_{i+\frac{1}{2},j,k}\right](q_{l-1})_{i+1,j,k} + \tfrac{1}{2}\left[(a_{l-1})_{i+\frac{1}{2},j,k}+(a_{l-1})_{i,j+\frac{1}{2},k}\right](q_{l-1})_{i,j+\frac{1}{2},k} + \tfrac{1}{2}\left[1-(a_{l-1})_{i,j+\frac{1}{2},k}\right](q_{l-1})_{i,j+\frac{1}{2},k}\,, \quad k=1,2,3,4. \tag{2.14d}$$

With for q the conservative state vector $q=(\rho,\rho u,\rho v,\rho e)^T$, the linear relations (2.14a)-(2.14d) approximately, but clearly display, how the upwind prolongation distributes mass, momentum and energy from a coarse grid to the overlying finer grid. For the approximately adjoint restriction operator (i.e. the approximation of the exact nonlinear adjoint), we can then write

$$\begin{aligned}(r_{l-1})_{i,j,k} = (I_l^{l-1} r_l)_{i,j,k} = {} & \tfrac{1}{2}\left[1-(a_{l-1})_{i-\frac{1}{2},j,k}\right]\left[(r_l)_{2i-2,2j-1,k}+(r_l)_{2i-2,2j,k}\right] + \\ & \tfrac{1}{2}\left[1-(a_{l-1})_{i,j-\frac{1}{2},k}\right]\left[(r_l)_{2i-1,2j-2,k}+(r_l)_{2i,2j-2,k}\right] + \\ & \tfrac{1}{2}(a_{l-1})_{i+\frac{1}{2},j,k}\left[(r_l)_{2i+1,2j-1,k}+(r_l)_{2i+1,2j,k}\right] + \\ & \tfrac{1}{2}(a_{l-1})_{i,j+\frac{1}{2},k}\left[(r_l)_{2i-1,2j+1,k}+(r_l)_{2i,2j+1,k}\right] + \\ & \tfrac{1}{2}\left[2-(a_{l-1})_{i-\frac{1}{2},j,k}-(a_{l-1})_{i,j-\frac{1}{2},k}\right](r_l)_{2i-1,2j-1,k} + \\ & \tfrac{1}{2}\left[1-(a_{l-1})_{i-\frac{1}{2},j,k}+(a_{l-1})_{i,j+\frac{1}{2},k}\right](r_l)_{2i-1,2j,k} + \\ & \tfrac{1}{2}\left[1+(a_{l-1})_{i+\frac{1}{2},j,k}-(a_{l-1})_{i,j-\frac{1}{2},k}\right](r_l)_{2i,2j-1,k} + \\ & \tfrac{1}{2}\left[(a_{l-1})_{i+\frac{1}{2},j,k}+(a_{l-1})_{i,j+\frac{1}{2},k}\right](r_l)_{2i,2j,k}\,, \quad k=1,2,3,4. \end{aligned} \tag{2.15}$$

Of course, the weak spot in (2.13)-(2.15) is the linear approximation of the nonlinear prolongation. In case $(q_{\text{face}})_k$ is a local extremum, i.e. does not lie in between $(q_{\text{left}})_k$ and $(q_{\text{right}})_k$, we have a negative coefficient in (2.13a) (either a_k or $1-a_k$), and hence also in (2.15). We do not accept this situation. If occurring, locally and for that k-th component only, we neglect how the upwind prolongation was, and simply take $(q_{\text{face}})_k = \frac{1}{2}((q_{\text{left}})_k + (q_{\text{right}})_k)$.

3. Results

We proceed by evaluating the novel techniques proposed. Instead of the multigrid results presented in Fig. 4, the multigrid results shown in Fig. 7 will be used as the starting point for improvement. The multigrid behaviour presented in Fig. 7 is obtained without nested iteration: q_l^0, $l=1,2,...,L$ are taken uniformly constant and equal to the hypersonic upstream boundary conditions. In this way we obtain a poorer initial approximation, but we have a more discriminating test problem, and we are ensured of an unambiguous evaluation, since q_l^0, $l=1,2,...,L$ will be the same for the different strategies to be considered.

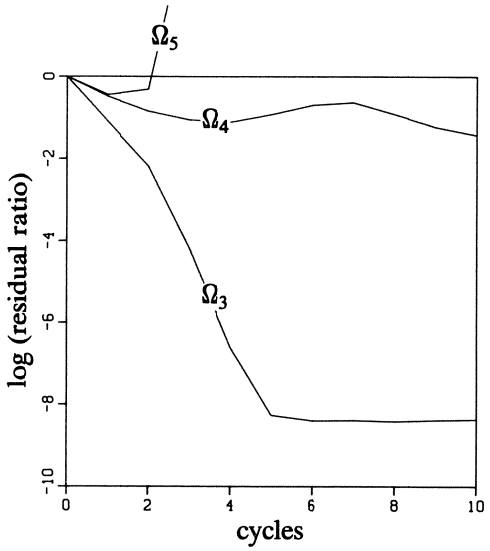

Fig. 7. Multigrid convergence behaviour blunt forebody with canopy at $M_\infty=8.15$, $\alpha=0^0$, without nested iteration, and without any novel multigrid constituent.

3.1. *With defect multiplication*

With the defect multiplication according to (2.8), damping only, we obtain the convergence results given in Fig. 8a. With the defect multiplication according to (2.9), both damping and amplification, we obtain the convergence results given in Fig. 8b. For the matrix norms, in both (2.8) and (2.9), we applied the Frobenius-like norm

$$\|(N_l')_{2i,2j}\| = 2^l \left[\Sigma_{k_1=1,k_2=1}^{4,4}(N_l')_{k_1,k_2}^2\right]_{2i,2j}^{\frac{1}{2}}, \tag{3.1}$$

the factor 2^{l-1} simply accounting for the fact that in our case $N_l(q_l)$ is a line integral form.

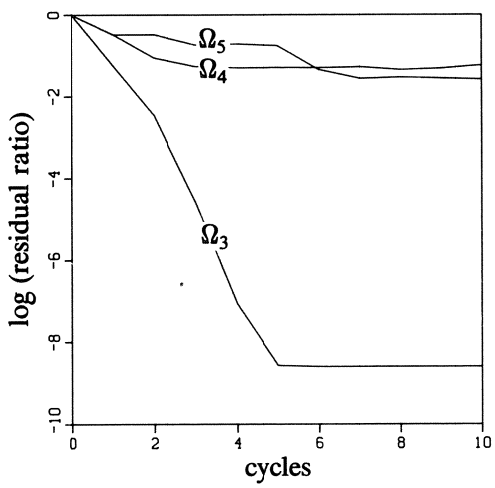

a. According to (2.8).

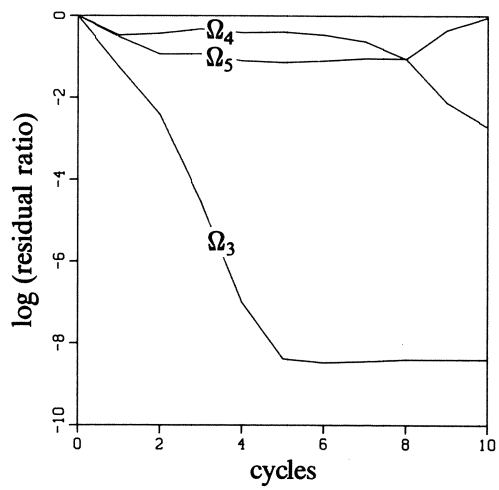

b. According to (2.9).

Fig. 8. Multigrid convergence behaviour blunt forebody with canopy at $M_\infty=8.15$, $\alpha=0^0$, with defect multiplication.

Corresponding to the results in Fig. 8a and 8b, in Fig. 9a and 9b we show distributions of the multiplication operator $S_{L-1},L=5$ (the multiplication factor distribution on Ω_4), as applied in the last (i.e. the 10-th) multigrid cycle. In both cases the local damping is confined to only the close neighbourhood of the blunt body. Locally, in Fig. 9b, the damping appears to be a little bit stronger than that in Fig. 9a. However, globally this is more or less compensated by the local amplifications. Notice that the maximal amplification factor that was found to be applied in Fig. 9b is only O(1). The minimal damping factors in Fig. 9a and 9b are much larger than those found by De Zeeuw [6] for his specific test case. A second difference with the results of De Zeeuw is the good improvement in [6] of the multigrid method's performance, and the modest present improvements. Both differences suggest that for the present test case, in order to significantly improve the results presented in Fig. 7, defect multiplication is not needed as much as improved grid transfers.

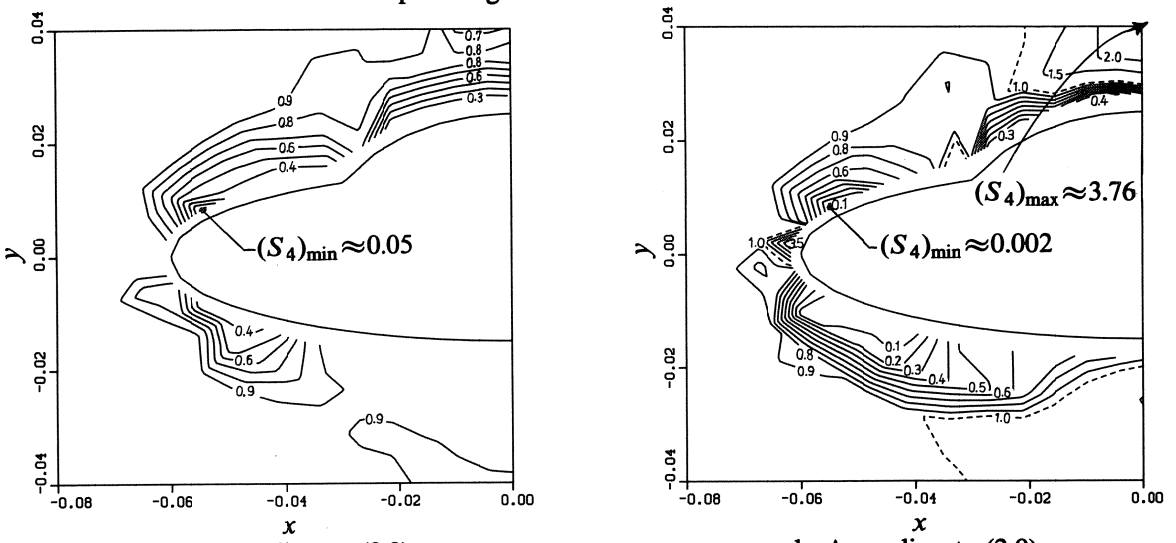

a. According to (2.8). b. According to (2.9).

Fig. 9. Distribution multiplication factors applied on Ω_4 in the 10-th multigrid cycle, blunt forebody with canopy at $M_\infty=8.15$, $\alpha=0^0$.

3.2. With direction-dependent grid transfer operators

The multigrid behaviour obtained after having replaced both the existing correction prolongation operator and the existing defect restriction operator by the direction-dependent operators, is given in Fig. 10a. (We notice that defect damping is not applied.) With better grid transfers only, the improvement with respect to Fig. 7 is significant indeed.

Replacing in the existing multigrid algorithm only the standard correction prolongation (by the upwind prolongation), we obtain the multigrid performance given in Fig. 10b. These results are even better than those in Fig. 10a, and hence make us conclude that the previous, somewhat cumbersome efforts in also upwinding the defect restriction, are not necessary.

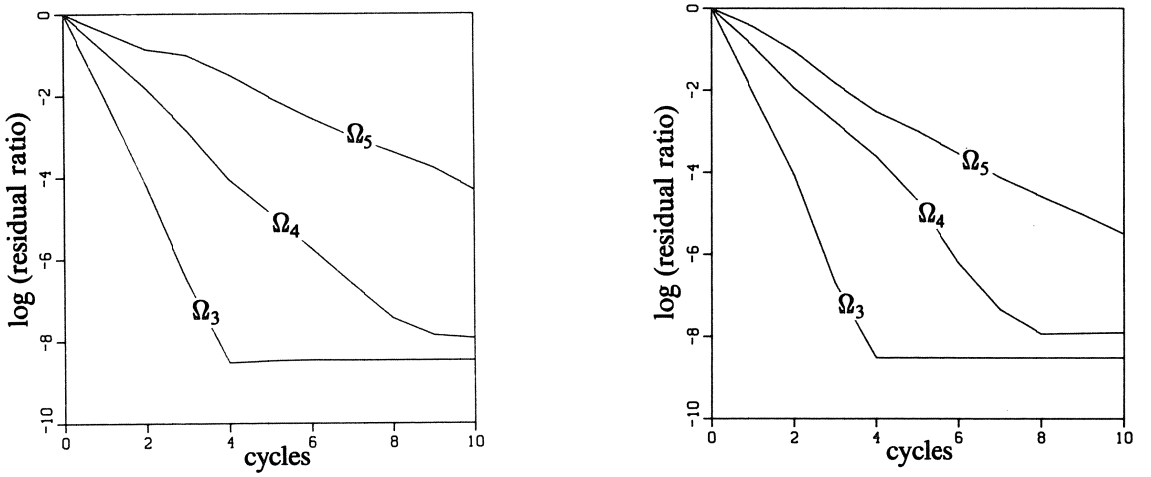

a. With upwind correction prolongation and upwind defect restriction. b. With upwind correction prolongation only.

Fig. 10. Multigrid convergence behaviour blunt forebody with canopy at $M_\infty=8.15$, $\alpha=0^0$.

3.3. With both defect damping and upwind correction prolongation

Though the two-grid convergence analysis in section 2.1 assumes that the prolongation operator is linear, see (2.4), no reason exists why local defect multiplication would have a detrimental effect in combination with the nonlinear upwind prolongation. Therefore, in the present section, we show the multigrid performance for the combination of both defect multiplication and upwind correction prolongation. Because the results in Fig. 8b already showed not to be better than those in Fig. 8a, and because of the potential danger for divergence which is inherent to the allowance for local defect amplification, in the following - for the defect multiplication - we will apply (2.8) only.

Combining both novel multigrid constituents as considered separately in the two previous sections, we obtain the multigrid results presented in Fig. 11. Comparison with the best of the previous results (Fig. 10b) learns that the combination of both techniques yields an even slightly better multigrid performance. We proceed in further investigating this favourite combination. In Fig. 12a we show the distribution of the operator $S_{L-1}, L=5$, as applied in the last (i.e. again the 10-th) multigrid cycle; a cycle in which the solution has already converged. First we notice that the damping has not vanished indeed. Further we notice that though the solution must be symmetrical around the front ellipse, the damping factor distribution is not. Cause of this is the fact that in the coarse grid problems, for the initial iterate, we take the latest iterate computed. (See e.g. the description of the nonlinear multigrid iteration in section 1.2, and more explicitly: equation (2.2).) By using the latest obtained iterate, the influence of the very first iterates is still felt, iterates which - due to their poor level of convergence - are not yet symmetrical around the front ellipse. An experimental proof of this explanation is given in Fig. 12b in which we show the converged damping factor distribution for a strategy *with* solution restriction. Here, the converged damping factor distribution around the front ellipse is clearly symmetrical indeed. Notice that in both Fig. 12a and Fig. 12b the applied damping is modest. In Fig. 12b - the case with solution restriction - it is even weaker than in Fig. 12a. However, taking the restriction of the solution on the coarser grids usually leads to a slower convergence than taking the latest available coarse grid iterates.

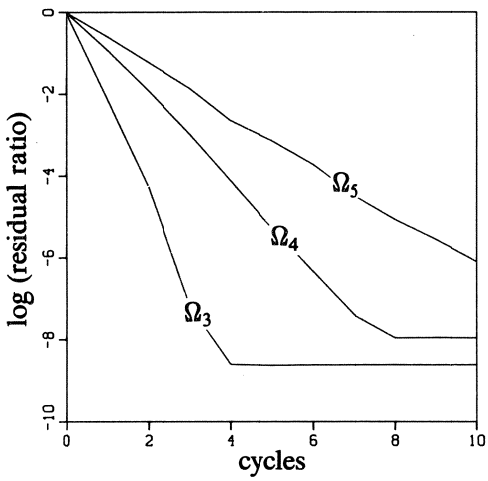

Fig. 11. Multigrid convergence behaviour,
blunt forebody with canopy at $M_\infty = 8.15$, $\alpha = 0^0$,
with both defect damping and upwind correction prolongation.

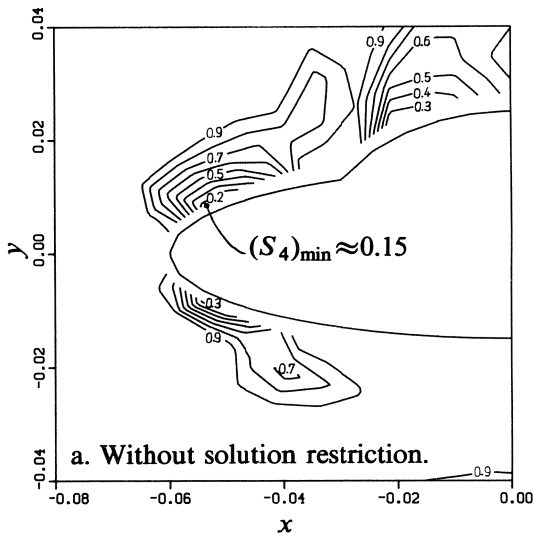

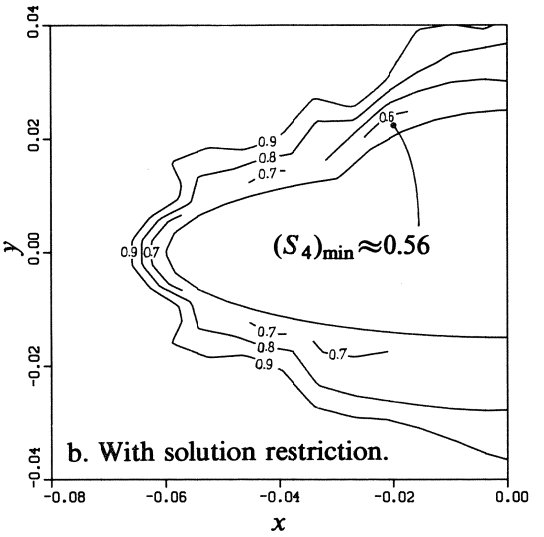

Fig. 12. Converged damping factor distributions on Ω_4,
blunt forebody with canopy at $M_\infty = 8.15$, $\alpha = 0^0$,
with both defect damping and upwind correction prolongation.

3.4. With both defect damping, upwind correction prolongation, and nested iteration

Comparison of the existing multigrid method's results presented in Fig. 4 and Fig. 7 - results obtained *with* and *without* nested iteration, respectively - clearly shows the natural beneficial influence of nested iteration. For the favourite multigrid strategy, the strategy with defect damping and upwind correction prolongation, the benefit of nested iteration (consistently, with upwind solution prolongation) is observed by counting the number of finite volumes in which - locally - the switch is made from the relaxation technique to the evolution technique (Fig. 13). In both Fig. 13a and 13b (without and with nested iteration, respectively), the quantity along the vertical axis is a scaled number of switches made during the n-th multigrid cycle ($n=1,2,...,10$), the scaling factor being the total number of volumes visited during one nonlinear multigrid cycle; a V-cycle with $p=q=1$, and with symmetric relaxation sweeps. (Notice that the scaling factor increases when going from Ω_3 to Ω_6.) The non-zero percentage at $n=0$ in Fig. 13b indicates the total amount of switches made during the nested iteration. For all four grids considered, the expected positive influence of the nested iteration appears to be significant. For both strategies the percentage of switches decreases with decreasing mesh size, which indicates that the difficulties are only of a local nature.

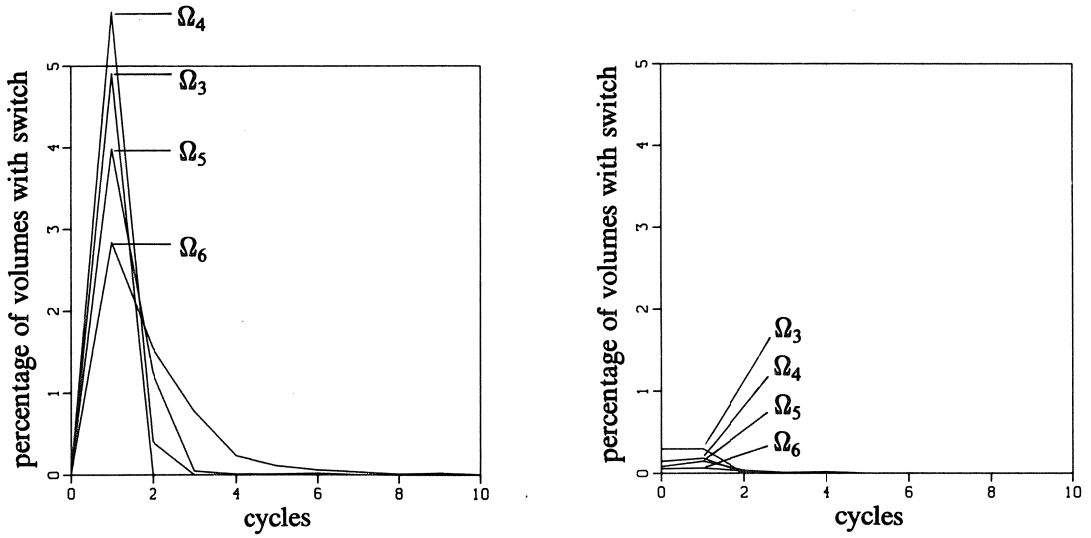

a. Without nested iteration.

b. With nested iteration.

Fig. 13. Amount of volumes with switch from relaxation to evolution, percentage of volumes visited during one multigrid cycle, blunt forebody with canopy at $M_\infty=8.15$, $\alpha=0^0$.

In Fig. 14 we give the convergence behaviour corresponding with the latest favourite strategy, the strategy with defect damping, upwind prolongation, and nested iteration. In this figure, for Ω_6, a comparison is also made with the corresponding single-grid convergence behaviour.

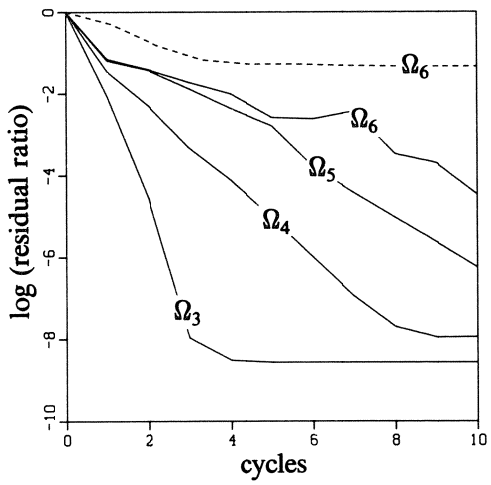

Fig. 14. Multigrid convergence behaviour blunt forebody with canopy at $M_\infty=8.15$, $\alpha=0^0$, with both defect damping, upwind prolongation, and nested iteration, (------ : single-grid, —— : multigrid).

In Fig. 15 we show a converged damping factor and Mach number distribution. Notice that the smallest damping factors are mainly concentrated along the bow shock, in particular there where the jumps across the shock are largest.

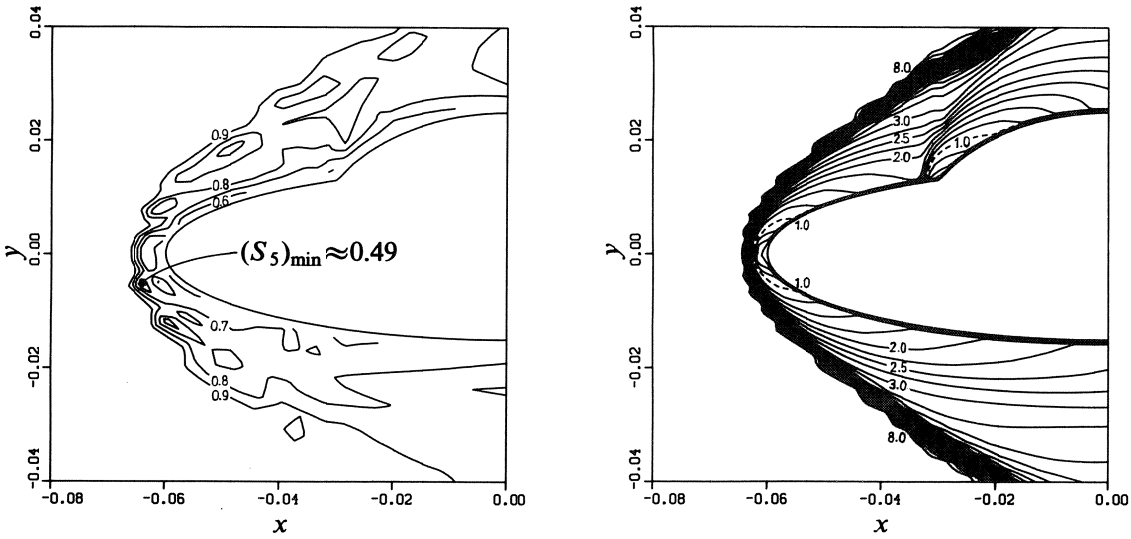

a. Damping factor distribution on Ω_5.

b. Mach number distribution on Ω_6.

Fig. 15. Converged results blunt forebody with canopy at $M_\infty = 8.15$, $\alpha = 0^0$, with both defect damping, upwind prolongation, and nested iteration.

Finally, we show results for the more interesting reentry case $M_\infty = 8.15$, $\alpha = 30^0$. Also for this test case, the convergence results (Fig. 16) show the beneficial influence of the changes in the existing multigrid method. Given the very low convergence rate of the single-grid computation (Fig. 16a), and given the absolute failure of the already existing multigrid method (both Fig. 16a and 16b), the novel multigrid constituents do not just appear to be a nice luxury, but a real necessity.

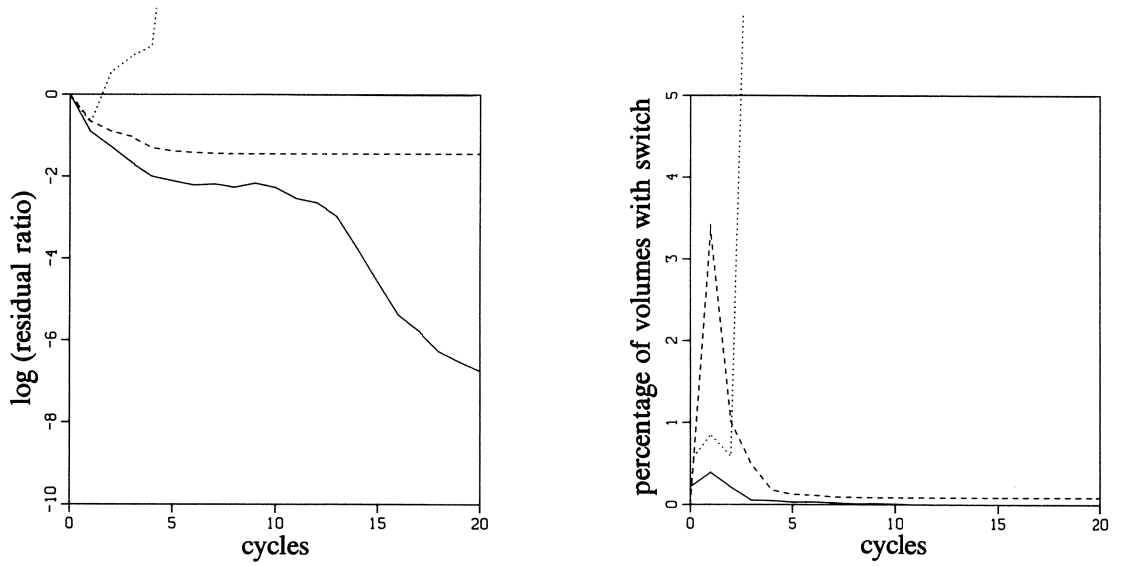

a. Convergence behaviour.

b. Amount of volumes with switch from relaxation to evolution, percentage of volumes visited during one multi-/single-grid cycle.

Fig. 16. Multigrid behaviour blunt forebody with canopy at $M_\infty = 8.15$, $\alpha = 30^0$, with both defect damping, upwind prolongation, and nested iteration, Ω_6 only, (------ : single-grid, ... : already existing multigrid, —— : novel multigrid).

Analogous to Fig. 15, in Fig. 17 we show a converged damping factor and Mach number distribution. Notice that - like in Fig. 15 - the smallest damping factors are located at the most pronounced part of the bow shock.

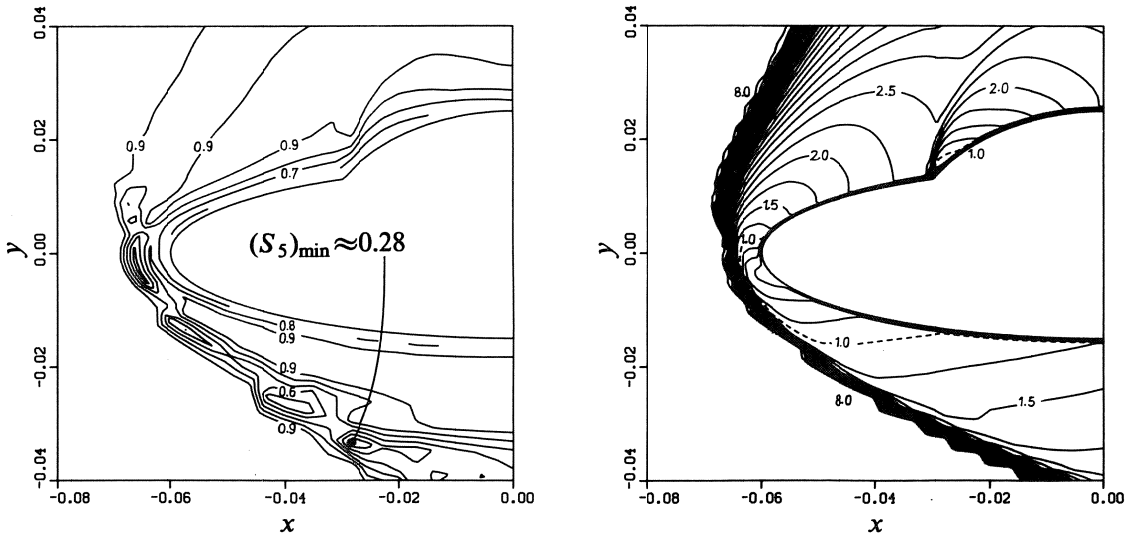

a. Damping factor distribution on Ω_5.

b. Mach number distribution on Ω_6.

Fig. 17. Converged results blunt forebody with canopy at $M_\infty = 8.15$, $\alpha = 30^0$, with both defect damping, upwind prolongation, and nested iteration.

Concerning the efficiency of the improved multigrid method, one may find the paradoxical result that one multigrid cycle with both defect damping and upwind correction prolongation is still cheaper than one multigrid cycle without both. The cause of this simply is that the computations with the improved multigrid method may result in a significantly smaller number of switches from the local relaxation to a local evolution during the smoothing phases, and hence in a lower computational cost. Concerning the efficiency of the upwind computation of cell face states (as applied in the upwind prolongation), for the test cases considered it appears that with the P-variant, at almost all cell faces it holds that $F(q_{\text{left}}, q_{\text{right}}) = f(q_*)$. (For both Ω_6-multigrid cases considered in this section, solving a quadratic equation for q_{face} appears to be necessary at about 1% of all cell faces only.)

To finish, we summarize the improved multigrid algorithm, the novel elements being indicated in bold.

Nested iteration:
- Choose q_1.
- Improve q_1 by a single nonlinear multigrid cycle.
- Transfer the improved approximation q_1 to Ω_2, **by applying the upwind prolongation operator.**
- Improve q_2 by a single nonlinear multigrid cycle.
- Continue the previous process until an initial estimate for q_L has been obtained by **upwind prolongation** of q_{L-1}.

Nonlinear multigrid iteration:
- Apply p pre-relaxation sweeps to $N_l(q_l) = r_l$.
- Compute the defect $d_l = N_l(q_l) - r_l$, and restrict it: $d_{l-1} = I_l^{l-1} d_l$.
- **Compute the local damping factors $(S_{l-1})_{i,j}$, and damp the restricted defect:** $d_{l-1} := S_{l-1} d_{l-1}$.
- Compute the right-hand side $r_{l-1} = N_{l-1}(q_{l-1}) - d_{l-1}$.
- Approximate the solution of $N_{l-1}(q_{l-1}) = r_{l-1}$ by the application of σ nonlinear multigrid cycles.
- Correct the current solution, **by applying the upwind prolongation operator.**
- Apply q post-relaxation sweeps to $N_l(q_l) = r_l$.

4. Conclusions

A satisfactory remedy against divergence of nonlinear multigrid in hypersonic flow computations appears to be the combination of a (local) damping of the restricted defect, and a (global) upwind prolongation of the correction. Besides a positive influence on the robustness of the algorithm, the combination of upwind prolongation and defect damping also has a positive influence on the computational efficiency. Both techniques are such that the improved algorithm still does not require any tuning of parameters.

References

[1] S.K. Godunov, Finite difference method for numerical computation of discontinuous solutions of the equations of fluid dynamics (Cornell Aeronautical Lab. Transl. from the Russian), *Math. Sbornik 47* (1959) 271-306.

[2] P.W. Hemker and S.P. Spekreijse, Multiple grid and Osher's scheme for the efficient solution of the steady Euler equations, *Appl. Numer. Math. 2* (1986) 475-493.

[3] B. Koren, Robustness improvement of point Gauss-Seidel relaxation for steady, hypersonic flow computations, *CWI-note NM-N8805,* Centre for Mathematics and Computer Science, Amsterdam (1988).

[4] S. Osher and F. Solomon, Upwind difference schemes for hyperbolic systems of conservation laws, *Math. Comput. 38* (1982) 339-374.

[5] A.A. Reusken, Convergence analysis of nonlinear multigrid methods, doctoral thesis, State University of Utrecht, Utrecht (1989).

[6] P.M. de Zeeuw, Nonlinear multigrid applied to a 1D stationary semiconductor model, *CWI-report NM-R8905,* Centre for Mathematics and Computer Science, Amsterdam (1989).